ChemistryEurope
Excellence in Chemistry Research Worldwide

Research Article
doi.org/10.1002/ceur.202500266

www.journal.chemistry-europe.org

Tracking Propagating Perturbations in Chemical Reactions

Charlotte Lefebvre and Quentin Duez*

Periodic perturbations, such as modulations of reactant concentration, propagate through chemical reactions with distinct phase delays. Tracking the propagation of such perturbations presents a powerful approach for probing the reaction connectivity and the rates of individual reaction steps, provided that high-throughput and information-rich analytical approaches are used. Here, the online monitoring of periodic perturbations in the organocatalytic addition of cyclopentadiene to α, β-unsaturated aldehydes by electrospray ionization–mass spectrometry (ESI–MS) is reported. Upon perturbation of input concentrations, ion intensities corresponding to substrates and reaction intermediates detected by ESI–MS exhibit characteristic time delays, providing insights into the kinetics of individual reaction steps, as supported by numerical simulations. This study provides a novel framework for online reaction monitoring and mechanistic analysis in chemical systems.

1. Introduction

Living systems adapt to perturbations in their environment via their underlying chemical reaction networks, which process and respond differently to external signals.[1] This behavior arises from an interplay between reaction kinetics and architectures, enabling dynamic responses. Taking inspiration from biological systems, a wide range of signal processing capabilities has been achieved with chemical reactions, ranging from the integrated response to periodic perturbations[2] to the execution of computational tasks by molecular input processing.[3]

Periodic perturbations, such as oscillating variations in reactant concentration,[2b,4] ac voltage or current,[5] or temperature[2c] propagate through chemical reaction networks. This is illustrated by a numerical simulation shown in **Figure 1**A, where a model reaction system in continuous flow conditions is subjected to a sinusoidal modulation of reactant concentration. The perturbation travels through the network, resulting in distinct phase delays and amplitude dampening in the concentration profile of other species, which are governed by the connectivity and kinetics of the individual steps.[6] For instance, Figure S1, S2, Supporting Information show the propagation of periodic concentration perturbations through idealized reaction networks with alternative architectures to that shown in Figure 1, while maintaining identical reaction rates. The resulting patterns demonstrate that the organization of reaction pathways strongly influences how perturbations propagate. Tracking the propagation of oscillating perturbations through chemical reaction networks can thus be a powerful approach to extract mechanistic information and obtain direct insights into reaction connectivity and rates.

This has been demonstrated in silico for idealized reaction systems[6] and experimentally for a limited number of reactions.[2,4] In the case of the formose reaction, for instance, modulating a reactant concentration and analyzing the amplitude responses of products by gas chromatography–mass spectrometry(MS) enabled to map out reaction pathways.[4] However, subtle temporal features such as small differences in phase delays ($\approx$s, min), are beyond the resolution of traditional low-throughput methods, thereby limiting the mechanistic insights that can be reached.

Generalizing this approach to a wide range of chemical reactions requires analytical approaches that combine a high throughput with extensive chemical observability, capable to capture concentration variations for many stable products and transient intermediates while maintaining sufficient temporal resolution. Electrospray ionization (ESI)–MS is well-suited for the online monitoring of complex reaction mixtures, as it enables the detection of individual compounds based on their mass-to-charge (m/z) ratios. Its high sensitivity and throughput enable the detection of elusive species such as reactive intermediates that are typically present at low concentrations in solution.[7] However, ESI–MS is not inherently quantitative because the ion abundances in the gas phase are affected by the ionization efficiency of their precursors, along with matrix effects arising from the analysis of crude reaction media.[7]

Here, we harness the interface between continuous flow chemistry and ESI–MS[8] to explore the propagation of periodic concentration perturbations in a continuous stirred-tank reactor (CSTR). The organocatalytic Michael-type addition of cyclopentadiene to α,β-unsaturated aldehydes (Figure 1B) was selected as a model reaction, as it is well documented[9] and all the intermediate species are detectable by ESI–MS.[10] Following the mechanism proposed by Hilgers et al.,[10a] this reaction proceeds

C. Lefebvre, Q. Duez
Organic Synthesis and Mass Spectrometry Laboratory
University of Mons
Place du Parc 23, 7000 Mons, Belgium
E-mail: quentin.duez@umons.ac.be

Supporting information for this article is available on the WWW under https://doi.org/10.1002/ceur.202500266

ChemistryEurope
Excellence in Chemistry Research Worldwide

Research Article
doi.org/10.1002/ceur.202500266

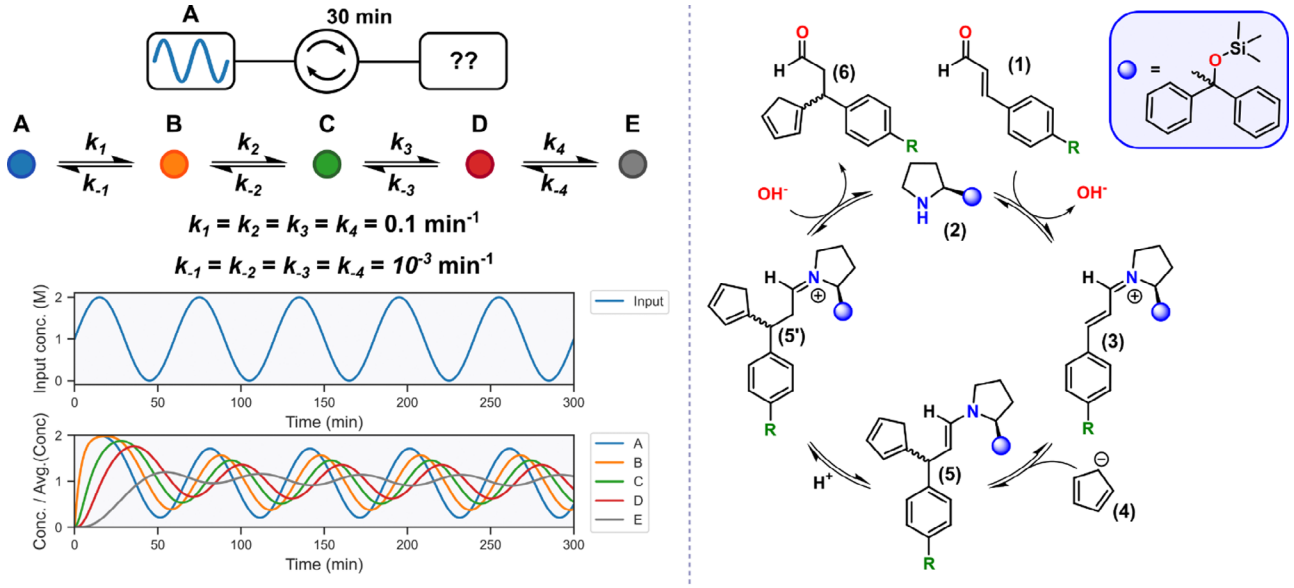

Figure 1. (Left) Numerical simulation of a model reaction system consisting of five compounds (A, B, C, D, and E) involved in four equilibria reactions with forward rate constants k_1, k_2, k_3, $k_4 = 0.1\ min^{-1}$ and reverse rate constants k_{-1}, k_{-2}, k_{-3}, $k_{-4} = 10^{-3}\ min^{-1}$. The numerical simulation is conducted in the conditions of a continuous stirred-tank reactor (CSTR), with average residence time $\tau = 30$ min. Modulations of the input concentrations of A result in the propagation of the oscillations to the concentrations of all other species. Additional details are provided in Supporting Information. (Right) Proposed reaction mechanism for the organocatalytic addition of cyclopentadiene to α,β-unsaturated aldehydes, adapted from Hilgers et al.[10a]

through the formation of a first iminium intermediate **(3)** by condensation between an α,β-unsaturated aldehyde **(1)** and a pyrrolidine derivative **(2)** acting as organocatalyst.[9,11] Michael-type addition of cyclopentadiene then results in an enamine intermediate **(5)** that can be protonated to yield a second iminium species **(5′)**. Hydrolysis of this final intermediate leads to the formation of the reaction product **(6)**. Experiments were performed with *para*-substituted aldehydes, referred to as **(1_H)**, **(1_{OMe})**, **(1_{Cl})**, **($1_{N(Me)2}$)**, and **(1_{NO2})**.

2. Results and discussion

We first examined the formation of the iminium intermediate **(3)** resulting from the condensation of **(1_{OMe})** and **(2)** under continuous flow conditions (**Figure 2**A). The reagents and solvent were stored in separate syringe pumps, each delivering a controlled flow rate to a CSTR (Figure 2B) mixed with a magnetic stirring bar. In this setup, the average residence time in the reactor ($\tau = 30$ min) is controlled by the total flow rate and reactor volume, while the individual inflows of reagents define the reaction conditions. The reactor outlet is directly connected to the ESI source of a mass spectrometer, allowing for online monitoring of the reaction medium. As shown in Figure 2C, the reagents **(1)** and **(2)** are respectively detected as sodiated $[\mathbf{1_{OMe} + Na}]^+$ and protonated $[\mathbf{2 + H}]^+$ ions or proton-bound dimers $[\mathbf{2_2 + H}]^+$, along with the proposed iminium species $[\mathbf{3}]^+$.

Following an initial steady state, the inflow of **(1_{OMe})** was modulated according to a sine wave function with a period of 120 min, resulting in periodic concentration perturbations in the reactor. To maintain a constant residence time, the inflow of solvent (MeOH) was dynamically adjusted to compensate for changes in the reagent flow rate. The ion intensities of the three species of interest were continuously monitored by ESI–MS, providing direct insights into the propagation of the input perturbation. As shown in Figure 2D, the input perturbation resulted in oscillations of ion intensities for all species monitored. Fitting the time courses with sine functions (Figure S3, Supporting Information) allowed us to determine both the phase delays and amplitudes of the observed oscillations. Of note, all experimental datasets were fitted both in the time and frequency domains. The resulting parameters can be found in Table S1–6, Supporting Information. This analysis revealed that the ion intensities of $[\mathbf{2 + H}]^+$ and $[\mathbf{3}]^+$ exhibit distinct time delays relative to the $[\mathbf{1_{OMe} + Na}]^+$ ions. The time delay between oscillations of $[\mathbf{1_{OMe} + Na}]^+$ and $[\mathbf{3}]^+$ was 9.1 min, while $[\mathbf{2 + H}]^+$ and $[\mathbf{3}]^+$ were found to oscillate with opposite phases. The opposite phase variations of $[\mathbf{2 + H}]^+$ and $[\mathbf{3}]^+$ directly relate to the underlying reaction mechanism, since the formation of each molecule of **(3)** requires the consumption of one molecule of **(2)**. Finally, the oscillation amplitudes of $[\mathbf{2 + H}]^+$ and $[\mathbf{3}]^+$ are found to be larger than $[\mathbf{1_{OMe} + Na}]^+$ (see Figure S3, Supporting Information).

To assess whether both time delays and oscillation amplitudes are relevant in the context of solution chemistry, we examined the concentration modulation of single compounds in a CSTR. When subjected to the same input perturbations, the oscillations amplitudes observed by ESI–MS vary significantly for different compounds (Figure S4, Supporting Information), suggesting that the ion intensity variations relate to concentration fluctuations in solution but depend also on the ionization efficiencies of individual compounds. On the other hand, the time delays between the observed oscillations should not depend on

ChemistryEurope
Excellence in Chemistry Research Worldwide

Research Article
doi.org/10.1002/ceur.202500266

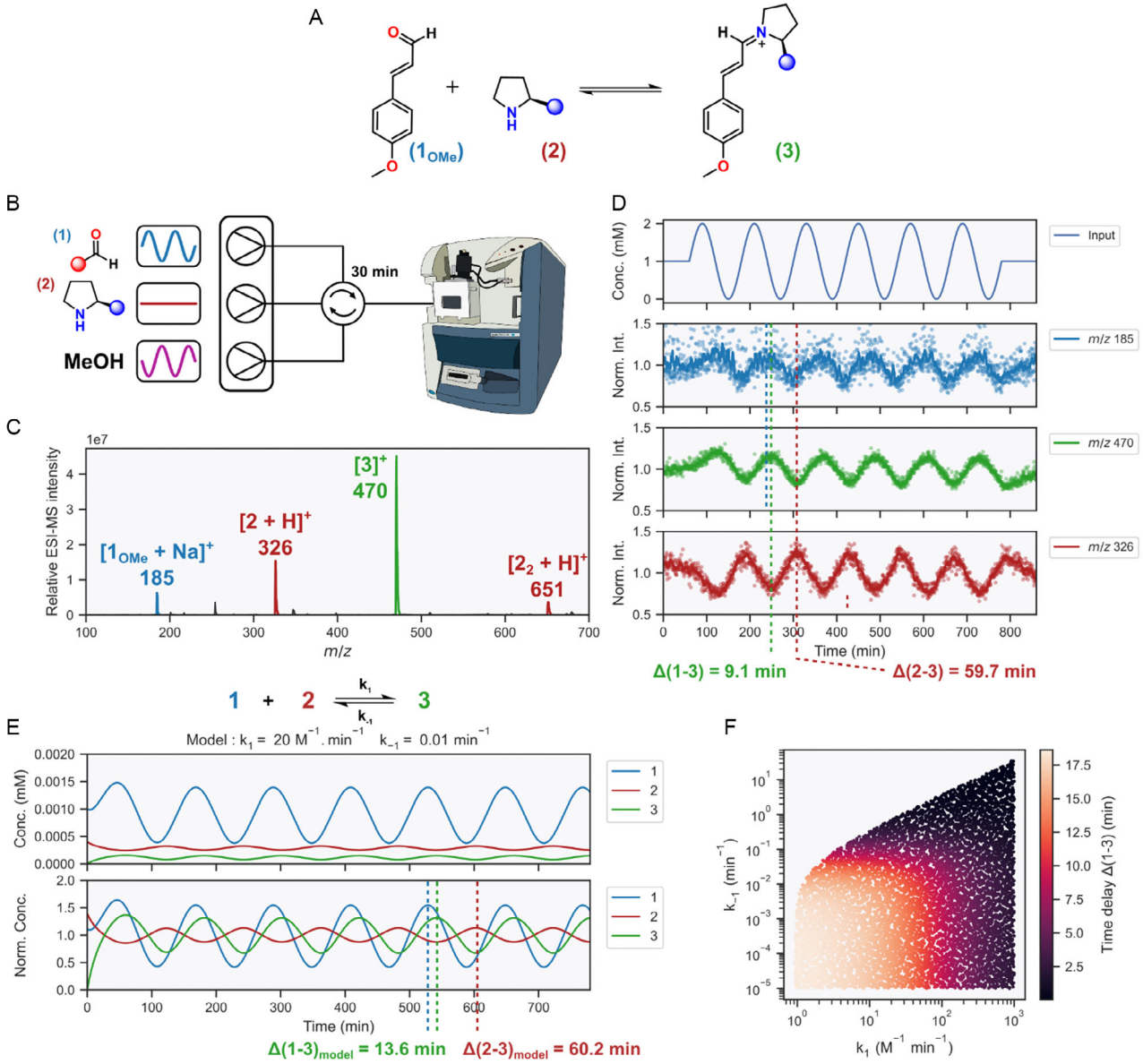

Figure 2. A) Formation of an iminium species by condensation of (**1**$_{OMe}$) and (**2**). B) Experimental setup interfacing a CSTR and an ESI–MS instrument. Three syringe pumps independently deliver the reagents (**1**$_{OMe}$), (**2**), and methanol. After an initial steady state, the flowrate of the syringe pump containing (**1**$_{OMe}$) is modulated according to a sine wave. To maintain the total flowrate constant and ensure a residence time of 30 min in the reactor, the flowrate of the solvent pump (MeOH) is dynamically adjusted. C) ESI–MS analysis of the reactor outflow. The reactants (**1**$_{OMe}$) and (**2**) are detected, along with an iminium species (**3**) resulting from the condensation reaction. D) Time course of ion intensities resulting from the input modulations of aldehyde concentration. Dots correspond to binned data, and lines correspond to rolling averages ($n = 10$). Ion intensities have been normalized by their mean value for better visualization. E) Model of a second order equilibrium reaction under oscillating input concentrations of (**1**). Concentrations obtained by solving the model with fixed k_1 and k_{-1} values are shown, along with normalized concentrations. F) Time delays between the species (**3**) and (**1**) obtained by solving the numerical model for many (k_1, k_{-1}) pairs. Additional details are provided in Supporting Information.

ionization efficiencies nor on matrix effects, making them a robust metric to probe reaction kinetics.

To better understand how the observed time delays relate to the underlying reaction kinetics, we considered a simple reaction model corresponding to the condensation reaction (Figure 2E). The model is based on the condensation of (**1**) and (**2**) into (**3**) with a forward rate constant k_1, whereas the reverse hydrolysis reaction takes place with a rate k_{-1}. Additional terms were incorporated into the rate equations to account for the continuous flow conditions and the oscillating aldehyde input concentration (see Supporting Information for model details). Numerical simulations were first performed with arbitrary rate constants ($k_1 = 20\ M^{-1}\ min^{-1}$ and $k_{-1} = 0.01\ min^{-1}$), yielding concentration time courses that closely resemble the experimental results. The model captures both the time delay between (**3**) and (**1**) $\Delta(1–3)_{model}$, predicted to be 13.6 min, and the opposite phase oscillations between (**2**) and (**3**) $\Delta(2–3)_{model}$, see Figure 2E.

Research Article
doi.org/10.1002/ceur.202500266

The impact of the rate constants on the predicted time delays between **(3)** and **(1)** was then evaluated by repeating the numerical simulations for more than 24,000 combinations of k_1 and k_{-1} sampled over a large parameter space. The resulting data shown in Figure 2F demonstrates that the time delay between oscillations of **(3)** and **(1)** depends on both k_1 and k_{-1}. As a result, filtering the modeled results for the experimentally observed time delay of 9.1 min (Figure 2D) yields many (k_1, k_{-1}) combinations, as shown in Figure S5, Supporting Information. This suggests that individual reaction rates cannot be directly obtained from the relative time delays alone. Nonetheless, these results indicate that phase relationships between the observed species constitute fingerprints of the reaction, enabling to confirm the proposed mechanism.

We next extended the reaction network by introducing cyclopentadiene **(4)** as an additional input, thereby enabling the Michael-type addition between **(4)** and **(3)** (**Figure 3**A). The experimental design was analogous to the one described in the previous paragraph, with the difference that the CSTR was heated to 40 °C to accelerate the addition reaction (Figure 3B). Continuous monitoring of the reactor outflow by ESI–MS enables the detection of the key species shown in Figure 2, along with the protonated iminium $[\mathbf{5'}]^+$ formed upon cyclopentadiene addition (Figure 3C). The final hydrolysis product **(6)** was not detected, suggesting that this step proceeds too slowly to yield a detectable amount within the 30 min residence time. Note that **[5]** and $[\mathbf{5'}]^+$ are treated as a single entity as the detected ions may either correspond to $[\mathbf{5'}]^+$ originating from the

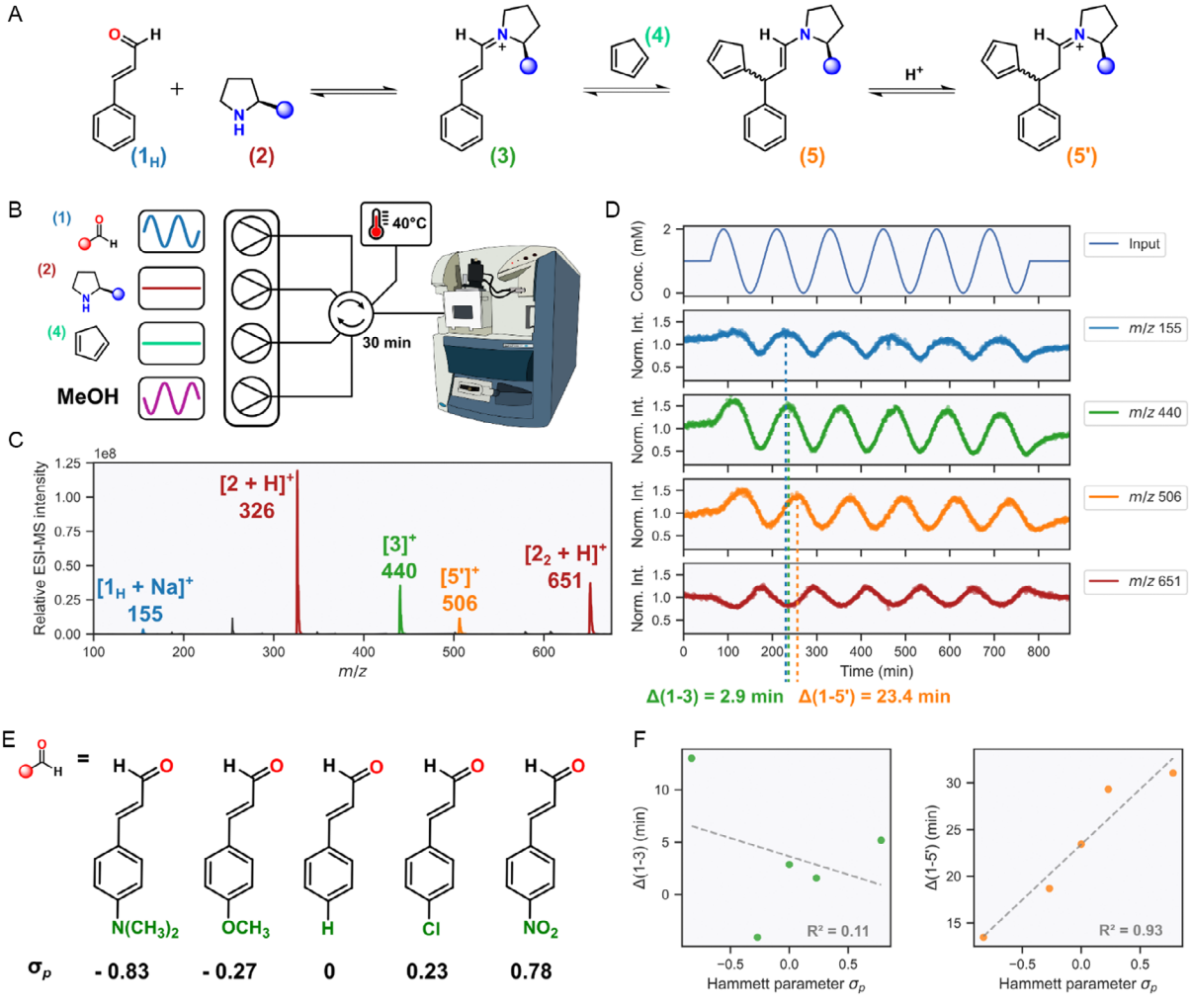

Figure 3. A) Formation of an iminium intermediate by condensation of **(1_H)** and **(2)**, followed by a Michael-type addition of **(4)**. B) Experimental setup interfacing a CSTR and an ESI–MS instrument. Syringe pumps independently deliver the reagents **(1_H)**, **(2)**, **(4)**, and methanol. After an initial steady state, the flowrate of the syringe pump containing **(1_H)** is modulated according to a sine wave function. To maintain the total flowrate constant and ensure a residence time of 30 min in the reactor, the flowrate of the solvent pump is dynamically adjusted. C) ESI–MS analysis of the reactor outflow. The reactants **(1_H)** and **(2)** are detected, along with iminium species resulting from the condensation reaction **(3)** and from the subsequent addition of cyclopentadiene **(5′)**. D) Time course of ion intensities resulting from the input modulations of aldehyde concentration. Dots correspond to binned data, and lines correspond to rolling averages ($n = 10$). The intensities have been normalized by their mean value for better visualization. E) Molecular structures and Hammett parameters of *para*-substituted α,β-unsaturated aldehydes. F) Correlation of the time delay between species **(3)** and **(1)** (Δ(1–3)) and **(5′)** and **(1)** Δ(1-5′)) with the Hammett parameter (σ_p). The time delays shown here are obtained by fitting the experimental data in the time domain. Grey dashed lines correspond to linear fits.

Research Article
doi.org/10.1002/ceur.202500266

solution, or arise from the protonation of **[5]** in the ESI source of the instrument.

Modulation of the aldehyde ($\mathbf{1_H}$) concentration following a sine wave function leads to periodic perturbations that propagate through the reaction network, evidenced by time-delayed oscillations in the ion intensities of $[\mathbf{3}]^+$ and $[\mathbf{5'}]^+$ relative to $[\mathbf{1} + \mathbf{Na}]^+$, respectively denoted Δ(1–3) and Δ(1-5′) (Figure 3D). Note that in experiments involving **(4)**, the large ion current of the protonated pyrrolidine derivative $[\mathbf{2} + \mathbf{H}]^+$ oversaturated the instrument detector and the proton-bound dimer of **(2)** ($[\mathbf{2_2} + \mathbf{H}]^+$) was monitored instead.

Because the relative time delays between propagating oscillations are proposed to reflect the reaction kinetics in solution, we next examined the effect of *para*-substituents on these delays. To this end, we repeated the experiment shown in Figure 3B with a series of four *para*-substituted cinnamaldehydes (Figure 3E; datasets in Figure S6-10, Supporting Information), with substituents ranging from strongly electron-donating (*p*-dimethylamino) to electron-withdrawing (*p*-nitro) groups. Substituent variation is expected to influence the reaction kinetics, as supported by batch conversion measurements for all five aldehydes (Figure S11,S12, Supporting Information); electron-withdrawing substituents lead to significantly higher conversion, consistent with a faster nucleophilic attack of cyclopentadiene **(4)** on the iminium intermediate **(3)**.

As shown in Figure 3F, Δ(1–3) showed no correlation with the Hammett parameter σ_p ($R^2 = 0.11$). In contrast, the strong correlation ($R^2 = 0.93$) observed between σ_p and Δ(1-5′) demonstrates that *para*-substituents have a direct impact on the Michael-type addition between **(3)** and **(4)**; electron-donating groups result in shorter delays, while electron-withdrawing groups exhibit longer Δ(1-5′). Hammett plots obtained by fitting ESI–MS data in the frequency domain can be found in Figure S13, Supporting Information and show a similar trend.

The longer Δ(1–5′) time delays observed for electron-withdrawing substituents are somewhat counterintuitive, as these substituents show significantly higher conversion. To rationalize the observed trends, we constructed a numerical model describing the reaction in continuous flow conditions (details in Supporting Information). The model considers the condensation of **(1)** with **(2)**, yielding a first intermediate **(3)**, which subsequently reacts with **(4)** to form **(5)**. Since the hydrolyzed products were not detected experimentally, this step was omitted in the model. The

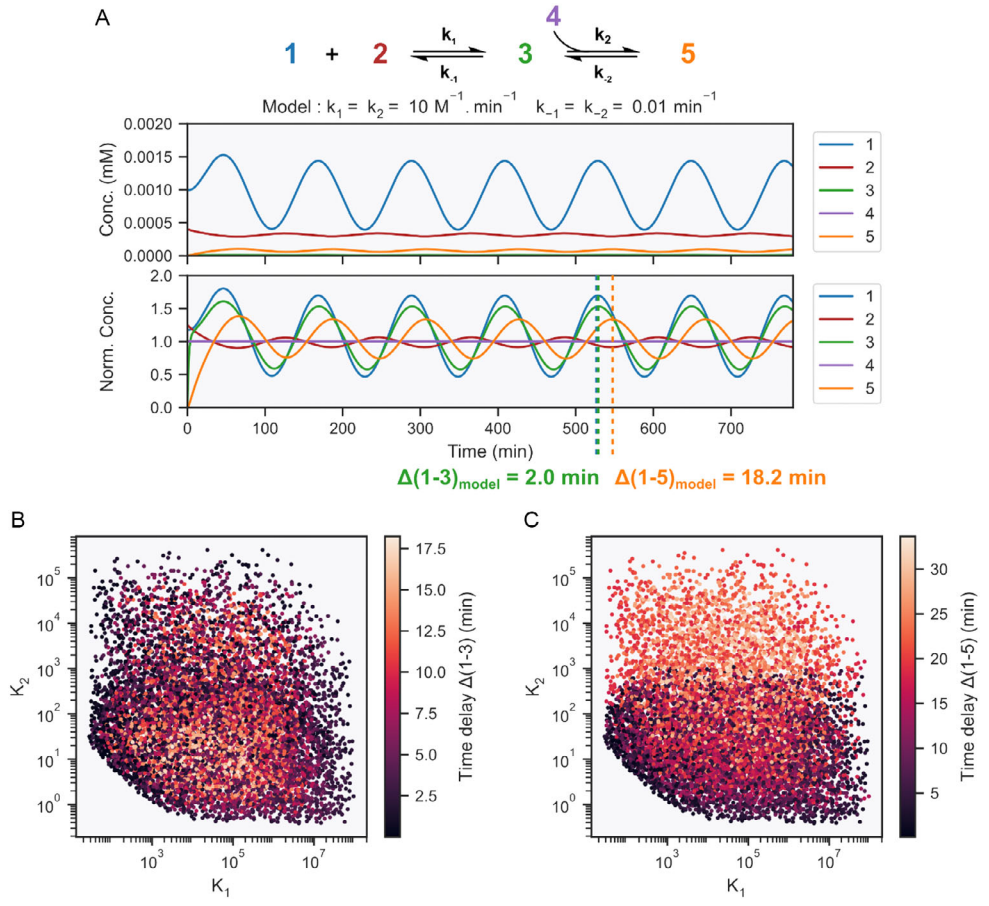

Figure 4. A) Model of two consecutive second order equilibrium reactions under oscillating input concentrations of **(1)**. Concentrations obtained by solving the model with fixed (k_1, k_{-1}, k_2, and k_{-2}) values are shown, along with normalized concentrations. B) Time delays between the species **(3)** and **(1)** obtained by solving the numerical model for many (k_1, k_{-1}, k_2, and k_{-2}) values, as a function of the equilibrium constants K_1 and K_2. Additional details are provided in Supporting Information. C) Time delays between the species **(5)** and **(1)** obtained by solving the numerical model for many (k_1, k_{-1}, k_2, and k_{-2}) values, as a function of the equilibrium constants K_1 and K_2. Additional details are provided in Supporting Information.

Research Article
doi.org/10.1002/ceur.202500266

two consecutive equilibria are characterized by forward rate constants k_1 and k_2 and reverse rate constants k_{-1} and k_{-2}, respectively. Solving the model for fixed (k_1, k_{-1}, k_2, and k_{-2}) values produces simulated concentration time courses shown in **Figure 4**A, which can be fitted with sine functions to yield the relative time delays between **(1)** and **(3)** $\Delta(1–3)_{model}$ and between **(1)** and **(5)** $\Delta(1–5)_{model}$. For arbitrarily selected rate constants ($k_1 = k_2 = 10\ M^{-1}.min^{-1}$; $k_{-1} = k_{-2} = 0.01\ min^{-1}$), $\Delta(1–3)_{model}$, and $\Delta(1–5)_{model}$, respectively, amount to 2 min and 18.8 min.

We next solved the numerical model for over 80,000 combinations of fixed rate constants (k_1, k_{-1}, k_2, and k_{-2}) to evaluate how the $\Delta(1–3)_{model}$ and $\Delta(1–5)_{model}$ values depend on the rate constants of individual reaction steps. Given the 4D nature of the parameter space, we simplified the analysis by focusing on the equilibrium constants K_1 and K_2 ($K_X = k_X/k_{-X}$). This allowed us to represent the modeled time delays $\Delta(1–3)_{model}$ and $\Delta(1–5)_{model}$ as a function of K_1 and K_2, as shown in Figure 4B,C. While $\Delta(1–3)_{model}$ does not show any correlation with K_1 and K_2, $\Delta(1–5)_{model}$ values are larger with growing K_2, regardless of K_1. The model thus suggests that large $\Delta(1–5)$ values are characteristic of strongly forward-driven reactions on the second step (Figure 4C), in good agreement with the larger time delays observed for electron-withdrawing substituents in Figure 3F.

3. Conclusion

In summary, tracking the propagation of periodic concentration perturbations through chemical reaction networks by ESI–MS is presented here as a powerful strategy for online reaction monitoring. The phase delays between key species provide insights into solution-phase kinetics, as demonstrated by probing substituent effects on the relative rates of individual reaction steps. The experimental observations are supported by numerical simulations, providing a blueprint for future mechanistic investigations on the impact of reaction conditions, such as substrate nature, solvent, or temperature, on the kinetics of individual reaction steps. This proof of concept paves the way for the analysis of large chemical reaction networks, which are often challenging to deconvolute with traditional analytical approaches.

Supporting Information

The authors have cited additional references within the Supporting Information.

Acknowledgements

This work was supported by a Fonds National de la Recherche Scientifique (FRS-FNRS) postdoctoral fellowship to Q.D. The UMONS MS laboratory acknowledges the FNRS for continuing support. Q.D. thanks Mr. Thijs de Jong for his help with designing the CSTR and Prof. Pascal Gerbaux for proof-reading the manuscript.

Conflict of Interest

The authors declare no conflict of interest.

Data Availability Statement

The data that support the findings of this study are openly available in [Zenodo] at [https://doi.org/10.5281/zenodo.16944279], reference number [16944279].

Keywords: continuous flow chemistry · kinetic modeling · mass spectrometry · online reaction monitoring · organocatalysis

[1] a) M. Samoilov, A. Arkin, J. Ross, *J. Phys. Chem. A.* **2002**, *106*, 10205; b) A. L. Barabasi, Z. N. Oltvai, *Nat. Rev. Genet.* **2004**, *5*, 101; c) M. Cloutier, P. Wellstead, *J. R. Soc. Interface* **2010**, *7*, 651.
[2] a) J. T. Mettetal, D. Muzzey, C. Gómez-Uribe, A. Van Oudenaarden, *Science* **2008**, *319*, 482; b) C. Urmès, J. Obeid, J.-M. Schweitzer, A. Cabiac, C. Julcour, Y. Schuurman, *Chem. Eng. Sci.* **2020**, *214*, 114544; c) O. R. Maguire, A. S. Y. Wong, M. G. Baltussen, P. van Duppen, A. A. Pogodaev, W. T. S. Huck, *Chem. Eur J.* **2020**, *26*, 1676.
[3] a) M. Ikeda, T. Tanida, T. Yoshii, K. Kurotani, S. Onogi, K. Urayama, I. Hamachi, *Nat. Chem.* **2014**, *6*, 511; b) N. M. Ivanov, M. G. Baltussen, C. L. F. Regueiro, M. T. G. M. Derks, W. T. S. Huck, *Angew. Chem. Int. Ed.* **2023**, *62*, e202215759.
[4] a) P. Müller, I. Hermans, *Ind. Eng. Chem. Res.* **2017**, *56*, 1123; b) W. E. Robinson, E. Daines, P. van Duppen, T. de Jong, W. T. S. Huck, *Nat. Chem.* **2022**, *14*, 623; c) J. Weyel, L. Schumacher, M. Ziemba, M. Pfeiffer, C. Hess, *Acc. Chem. Res.* **2024**, *57*, 2643; d) L. Brandão, E. A. High, T.-S. Kim, C. Reece, *Chem. Eng. J.* **2023**, *478*, 147489.
[5] a) T. Vidaković-Koch, T. Miličić, L. A. Živković, H. S. Chan, U. Krewer, M. Petkovska, *Curr. Op. Elect.* **2021**, *30*, 100851; b) A. C. Lazanas, M. I. Prodromidis, *ACS Meas. Sci. Au* **2023**, *3*, 162.
[6] R. Roszak, M. D. Bajczyk, E. P. Gajewska, R. Hołyst, B. A. Grzybowski, *Angew. Chem.* **2019**, *131*, 4568.
[7] a) M. Pahl, M. Mayer, M. Schneider, D. Belder, K. R. Asmis, *Anal. Chem.* **2019**, *91*, 3199; b) J. Mehara, J. Roithová, *Chem. Sci.* **2020**, *11*, 11960; c) O. J. Shiels, M. Menti-Platten, F. R. B. Bokosi, B. R. Burns, S. T. Keaveney, P. A. Keller, P. J. Barker, A. J. Trevitt, *Anal. Chem.* **2023**, *95*, 15472.
[8] Q. Duez, *Chem.–Methods* **2025**, *5*, e202400036.
[9] a) H. Gotoh, T. Uchimaru, Y. Hayashi, *Chem. Eur. J.* **2015**, *21*, 12337; b) T. M. Brauer, Q. Zhang, K. Tiefenbacher, *J. Am. Chem. Soc.* **2017**, *139*, 17500.
[10] a) R. Hilgers, S. Y. Teng, A. Bris, A. Y. Pereverzev, P. White, J. J. Jansen, J. Roithová, *Angew. Chem.* **2022**, *61*, e202205720; b) M. A. Hellinghuizen, P. Franceschi, J. Roithová, *Chem. Eur J.* **2024**, *30*, e202400294.
[11] a) K. A. Ahrendt, C. J. Borths, D. W. C. MacMillan, *J. Am. Chem. Soc.* **2000**, *122*, 4243; b) T. M. Bräuer, Q. Zhang, K. Tiefenbacher, *Angew. Chem. Int. Ed.* **2016**, *55*, 7698.

Manuscript received: July 12, 2025
Revised manuscript received: August 25, 2025
Version of record online: